Modeling and Analysis of Capacitive Wireless Power Transfer Systems: A Network Approach

Eli Abramov, *Student Member*, *IEEE*, and Mor Mordechai Peretz, *Member*, *IEEE*
The Center for Power Electronics and Mixed-Signal IC, Department of Electrical and Computer Engineering
Ben-Gurion University of the Negev, P.O. Box 653, Beer-Sheva, 8410501 Israel
eliab@post.bgu.ac.il, morp@ee.bgu.ac.il
http://www.ee.bgu.ac.il/~pemic

***Abstract*—This paper introduces a two-port network based approach to model capacitive wireless power transfer systems. A simple, generic and unified model to describe capacitive WPT system, under variations has been developed. The behavioral model and methodology have been validated through simulations and experiments. A 75W experimental capacitive WPT prototype has been designed and examined for various operating conditions, at switching frequency of 1.55MHz. A very good agreement is obtained between the theoretical behavioral model predictions, simulations, and measured experimental results.**

Keywords—behavioral modelling, capacitive power transfer, capacitive coupling, gyrator, matching networks, two-port network.

I. Introduction

Over the last few years, capacitive power transfer (CPT) is a rapidly growing technology in the field of wireless power transfer (WPT) [1]-[6]. One of the more attractive advantages of capacitive-based WPT is the avoidance of undesired Eddy currents and electromagnetic interfaces (EMI) that comes with magnetic based WPT methods [7]-[9]. In addition to efficiency improvements, CPT systems are potentially with lower volume and construction complexity [1]-[6]. However, the power transfer capability and efficiency still depends on the distance and alignment between the transmitting and receiving sides, which is an inherent feature of near-field WPT systems [10] ,[11].

Several explorations and remedies for extended range power transfer are covered in the literature [12]-[15], for general and capacitive power transfer. An important step in the development of both uniform and specific solutions for extended range WPT systems is a generalized description of the energy transfer mechanism. This requires description of the transfer medium, circuit behavior and their interaction. In particular, in case that active compensation is added, a description of the system's dynamic response is essential. On the topic of magnetic field based WPT, there can be found several through circuit and system analyses, however, a generic behavioral model and modeling methodology for CPT has not been addressed to-date.

A simplified block diagram of a descriptive CPT system is shown in Fig. 1. In a similar way to magnetic field approaches, reactive networks on both the primary and secondary sides are used for impedance matching between the source and load characteristics [13]-[15]. To achieve degrees of freedom in terms of design, performance and overall input-output relationships in any WPT system, high-order matching networks are used [2], [15], [16]. Analysis of such high-order networks can be quite complex and tedious. As a result, the intricate interaction between the system parameters and characteristics may be overlooked or even missed. Several approaches have been employed to decipher the operation of high-order resonant structures such as: analytical multivariable matrices manipulations, geometrical representations [17], [18], and averaging [19], [20]. Circuit derivation of CPT by super-positioning theorem [2], [4], [6], [21] provides clear closed-form expressions to the power delivery and other important relationships. However, since some approximations are involved, accurate overall description not always obtained, in particular for description of the dynamic characteristics. Numerical simulations are also a strong tool to evaluate and characterize different resonant circuits, this approach however, losses generality and may be time-consuming for cases that a time domain cycle-by-cycle simulation is carried out [22]- [24]. It would be extremely beneficial if a simple and unified generic averaging behavioral modeling methodology for capacitive-based WPT systems is utilized.

The objective of this study is therefore to introduce a network-based approach to describe the behavior of capacitive WPT system, under variations of the source and the load circuits, coupling interface and matching networks. The modeling methodology results in a unified model for CPT that provides an insight to the cross-coupling relationship between the input and output parameters, and enables to account for changes in distance and alignment of the coupling plates.

The rest of the paper is organized as follows: Following a brief survey of WPT matching structures, Section II details the two-port network based analysis. Section III delineates a case study of a network based approach to analyze a CPT system. Experimental validation of the behavioral model is provided in Section IV. Section V concludes the paper.

II. Review: Two-Port Representation of Matching Networks

A. Matching Networks

Fig. 2 shows several popular matching network structures that are mostly used in capacitive WPT systems [1]-[6]. A well-known and simple option is depicted in Fig. 2a in which a series inductance connects to the coupling capacitance of the wireless medium and forms a resonator [1]. By this, operation in the vicinity of the resonant frequency results in efficient power transfer to the load. However, a significant drawback of this configuration is that changes either in the

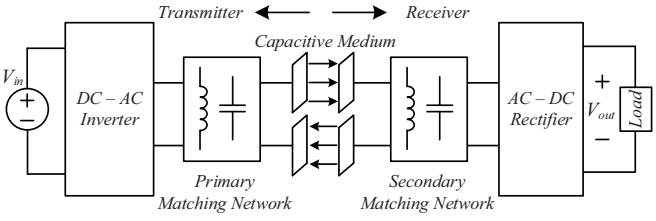

Fig. 1. Typical diagram of capacitive WPT system.

978-1-5386-6054-6/18/$31.00 ©2018 IEEE

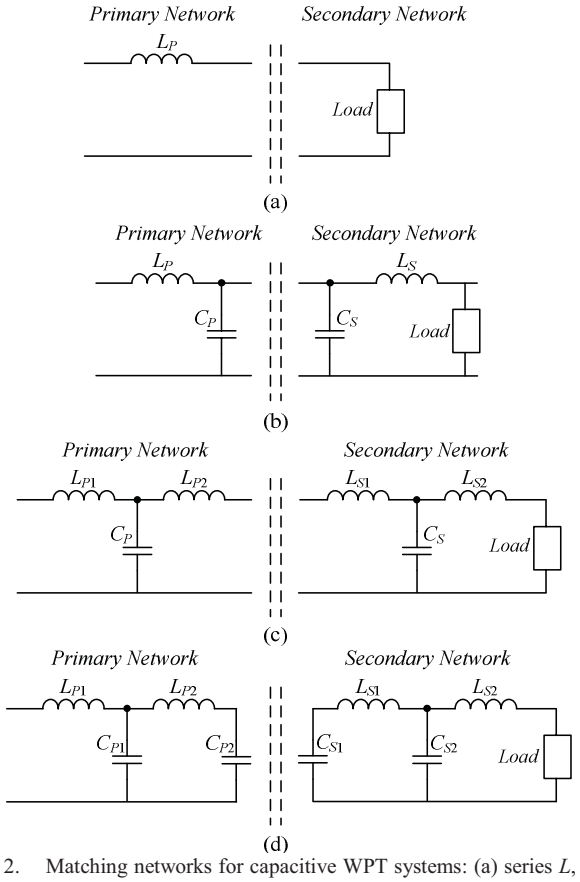

Fig. 2. Matching networks for capacitive WPT systems: (a) series *L*, (b) double-sided *LC*, (c) double-sided *LCL*, (d) double-sided *LCLC*.

capacitive medium or the load parameters, even the slightest, results in different operating point and a significant deterioration of the system ability to transfer power. This is somewhat alleviated by the configuration in Fig. 2b, in which both the primary and secondary sides of the coupling element include series-parallel resonators (Double-Sided *LC*). Here, the operating frequency is near the matching network's resonance, and therefore the system is less sensitive variations in the coupling capacitance (due to distance or misalignment variations). At the cost of slightly higher component count, the power transfer capabilities are higher than series compensation, but still depends on the coupling for efficiency and delivered power [4], [6]. The structure in Fig. 2c is a combination of the *LC* matching network with an additional series inductor on both sides of the system (Double-Sided *LCL*). By proper design of the inductors (L_P, L_{P1}, L_S, L_{S1}), this setup allows several degrees of freedom to adjust the power transfer of the system. However, as in the case of *LC* matching network, the power transfer capabilities of *LCL* structure is inversely proportional to the coupling capacitance [1], [3]. A more complex matching network is shown in Fig. 2d. It consists of a larger number of reactive elements on both primary and secondary (Double-Sided *LCLC*). There, the coupling capacitance in this case does not directly influence the resonance of the matching networks, it is however, still limits the amount of power transfer of the system, i.e. the lower the coupling capacitance is, proportionally lower the maximum power the system is able to transfer [2].

B. Equivalent Representations of Matching Networks

Matching L-type structures such as series inductor combined with parallel capacitor (series-parallel *LC*, Fig. 2b) and parallel capacitor combined with series inductor

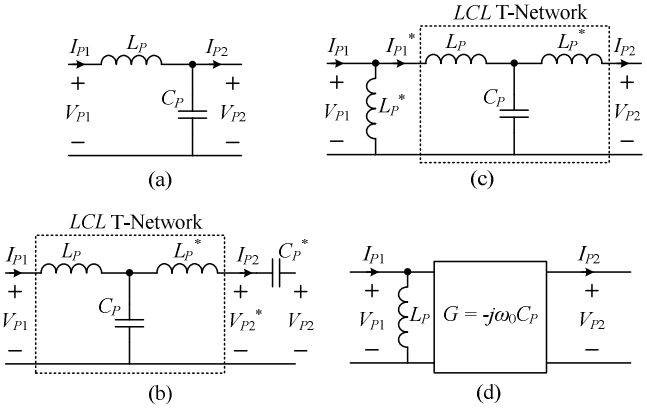

Fig. 3. Equivalent representations of series-parallel *LC* matching network: (a) L-type series-parallel resonant *LC* circuit; (b) Series resonator connected to the L-type circuit for T-type network arrangement; (c) Modified T-type series-parallel *LC* resonant circuit; (d) Two-port representation of the original L-type network.

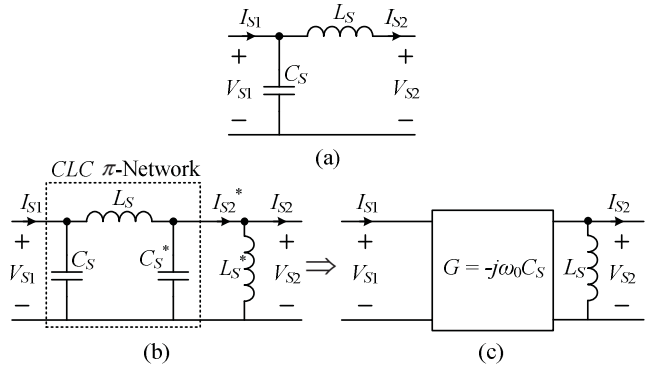

Fig. 4. Equivalent representations of parallel-series *LC* matching network: (a) L-type parallel-series resonant *LC* circuit; (b) Parallel resonator connected to the L-type circuit for π-type network arrangement; (c) Two-port representation of the original L-type network.

(parallel-series *LC*, Fig. 2b) can be described by a two-port network with gyrator characteristics [25]. A gyrator is a passive, lossless, linear two-port transformation network in which the output and input currents depend on the input and output voltages, respectively, with respect to its trans-conductance gain *G*. In circuit theory, gyrators often used to reflect inductance using capacitance, resistance into admittance, and vice versa [26], [27]. The input-output relationship of an ideal gyrator as a two-port network can be expressed as

$$\begin{bmatrix} I_1 \\ I_2 \end{bmatrix} = \begin{bmatrix} 0 & -G \\ G & 0 \end{bmatrix} \begin{bmatrix} V_1 \\ V_2 \end{bmatrix}. \tag{1}$$

In the context of the above discussion, voltage and current relationships of a series-parallel *LC* matching structure (Fig. 3a) can be derived as follows

$$\begin{cases} V_{P1} = j\omega L_P I_{P1} + V_{P2} \\ V_{P2} = \dfrac{1}{j\omega C_P}\left(I_{P1} - I_{P2}\right) \end{cases} \Rightarrow \begin{cases} I_{P1} = \dfrac{\left(V_{P1} - V_{P2}\right)}{j\omega L_P} \\ V_{P1} = j\omega L_P I_{P1} + \dfrac{1}{j\omega C_P}\left(I_{P1} - I_{P2}\right) \end{cases}. \tag{2}$$

Assuming operation at the resonant frequency, the currents I_{p1} and I_{p2} are given by

$$\begin{cases} I_{P1} = -j\omega_0 C_P \left(V_{P1} - V_{P2}\right) \\ I_{P2} = -j\omega_0 C_P V_{P1} \end{cases} ; \quad \omega_0 L_P = \frac{1}{\omega_0 C_P}, \tag{3}$$

where ω_0 is the resonant angular frequency.

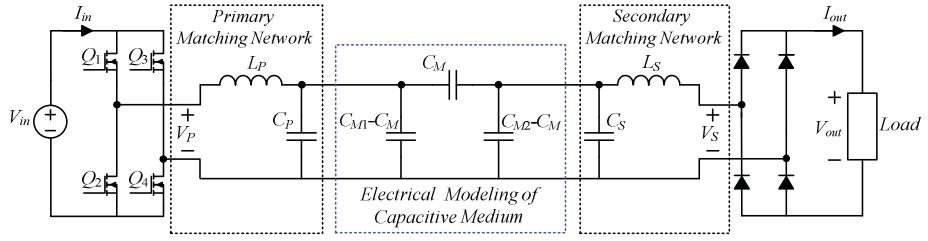

Fig. 5. Schematic diagram of a double-sided *LC* capacitive WPT system.

Employing few configurational modifications to the L-type network of Fig. 3a, an equivalent representation can be obtained. As can be seen in Fig. 3b, by addition of a series resonator (whereas $L_P^* = L_P$ and $C_P^* = C_P$) the network is transformed into a T-type one (L_P-C_P-L_P^*) with an output series capacitance C_P^*. The resultant voltage and current relationships have a two-port gyrator characteristics as follows

$$\begin{aligned} V_{P1} &= j\omega_0 L_P I_{P1} + \frac{1}{j\omega_0 C_P}\left(I_{P1} - I_{P2}\right) = \frac{1}{-j\omega_0 C_P} I_{P2} \\ V_{P2}^* &= -j\omega_0 L_P I_{P2} + \frac{1}{j\omega_0 C_P}\left(I_{P1} - I_{P2}\right) = \frac{1}{j\omega_0 C_P} I_{P1} \end{aligned}, \tag{4}$$

and in a matrix representation, (4) can be written as

$$\begin{bmatrix} I_{P1} \\ I_{P2} \end{bmatrix} = \begin{bmatrix} 0 & \underbrace{j\omega_0 C_P}_{-G} \\ \underbrace{-j\omega_0 C_P}_{G} & 0 \end{bmatrix} \begin{bmatrix} V_{P1} \\ V_{P2}^* \end{bmatrix}, \tag{5}$$

where the trans-conductance gain is $G = -j\omega_0 C_P$. It should be noted that assuming operation in resonance, the addition of the series branch is effectively short circuit and does not change the behavior of the circuit.

With the aid of the obtained gyrator relationships, the series output capacitance C_P^* can be reflected to an input parallel inductance L_P^*, as shown in Fig. 3c. Finally, the original L-type network can be represented as a gyrator element (Fig. 3d) with parallel input inductance L_p.

In analogy to the above practice for the series-parallel *LC* matching network, the parallel-series *LC* structure in Fig.4a can also be defined by gyration ratio. This is facilitated by addition of a parallel resonator (whereas $L_P^* = L_P$ and $C_P^* = C_P$) as shown in Fig.4 b. Similar to the case of the series branch, the parallel resonator is effectively open circuit when operating at resonance and does not change the original characteristics of the circuit. The L-network is transformed into a π-type one (C_S-L_S-C_S^*) with parallel output inductor L_S^*. The parallel-series *LC* structure can be described as a gyrator element with parallel output inductor L_S as shown in Fig.4 c.

III. Case Study: Capacitive Wireless Power Transfer System

Using the above observations, a capacitively coupled power transfer system with double-sided L-type matching networks is analyzed. Schematic diagram of the full system is shown in Fig. 5, which has been widely considered in variety of medium power level CPT applications [4], [6], [28]. As can be seen, the matching network in the primary side is a series-parallel *LC* circuit and the matching network at the secondary is a parallel-series *LC*. The capacitive medium is equivalently modeled by a π-network, such that C_M is the equivalent mutual capacitance and C_{M1} and C_{M2} are the self-capacitances of the coupling plates [3], [4], [6]. The system is driven by a full-bridge inverter on the primary side, and the load is fed via a diode rectifier that is connected to the secondary's network. Considering that the coupling capacitance C_M is significantly lower than the total parallel capacitance and that the drive frequency is near the matching networks' resonant frequency (i.e., $f_0=(2\pi\sqrt{L_P C_P})^{-1} =(2\pi\sqrt{L_S C_S})^{-1}$), the currents as well as voltages of the reactive elements are virtually sinusoidal. This is since high-Q operation is naturally facilitated as the output impedance of the primary's network is relatively high.

The circuit of Fig. 5 is simplified by separating the parallel capacitances of the medium model to self-capacitances as shown in Fig. 6a. This forms a π-network constructed by the mutual capacitance C_M, which can be analyzed similarly to the *CLC* π-matching network from Section II. This yields a gyrator element to represent the coupling behavior as depicted in Fig. 6b. In the context of the overall system, Fig. 5 is simplified as delineated in Fig. 6c. Assigning the network dualities that have been established earlier, the entire system is represented by three gyrators connected in series (Fig. 6d; $C_P^* = C_P + C_{M1}$ and $C_S^* = C_S + C_{M2}$; C_P, $C_S >> C_{M1}$, C_{M2}). This is further reduced to a single gyrator, as illustrated in Fig. 6e, with total trans-conductance gain that can be expressed as

$$G_{total} = \frac{j\omega_0 C_P^* C_S^*}{C_M}. \tag{6}$$

The simplified circuit of the double-sided *LC* capacitive WTP system in Fig. 6e can be now analyzed in a straightforward approach as a two-port network with gyrator characteristics, such that the current-voltage relationships are expressed as follows

$$\begin{aligned} I_P &= \frac{V_P}{j\omega_0 L_P} - \frac{j\omega_0 C_P^* C_S^*}{C_M} V_S = -j\left(\frac{V_P}{\omega_0 L_P} + \frac{\omega_0 C_P^* C_S^*}{C_M} V_S\right) \\ I_S &= -\frac{V_S}{j\omega_0 L_S} + \frac{j\omega_0 C_P^* C_S^*}{C_M} V_P = j\left(\frac{V_S}{\omega_0 L_S} + \frac{\omega_0 C_P^* C_S^*}{C_M} V_P\right) \end{aligned}. \tag{7}$$

In typical operation of such CPT applications, the operating frequency is in the MHz range, the networks' parallel capacitance values are in the range of 100s pF, inductances at μH, and the mutual coupling capacitance, C_M, is in the order of few pF. As a result, the transfer relationship of the system can be simplified to generic expressions as follows

$$\begin{aligned} I_P &= \frac{\omega_0 C_P^* C_S^*}{C_M} V_S \\ I_S &= \frac{\omega_0 C_P^* C_S^*}{C_M} V_P \end{aligned} \quad ; \quad \begin{cases} \dfrac{\omega_0 C_P^* C_S^*}{C_M} >> \dfrac{1}{\omega_0 L_{P/S}} \\ G \approx G_{total} = \dfrac{\omega_0 C_P^* C_S^*}{C_M} \end{cases}, \tag{8}$$

which is in excellent agreement with [4] and [6].

The implication of this analysis is that the double-sided *LC* capacitive WPT system can be modeled as a voltage-dependent current source as illustrated in Fig. 7. Employing

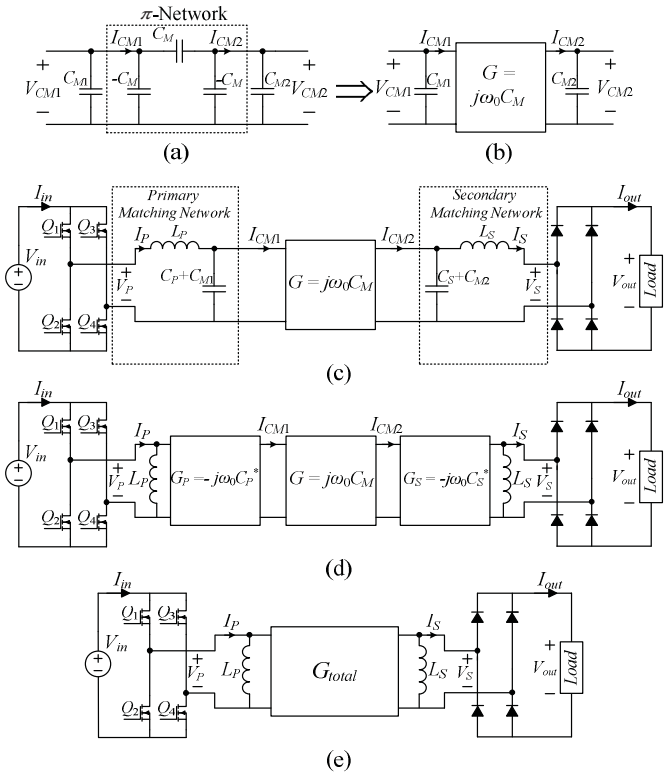

Fig. 6. Equivalent two-port network based models of the analyzed capacitive WPT system: (a) Electrical equivalent model of four-plate capacitive medium; (b) Representation of the capacitive medium with a two-port network; (c) Representation of double-sided *LC* capacitive WPT system with a gyrator as the capacitive medium; (d) Equivalent circuit of double-sided *LC* capacitive WPT system with three series gyrators; (e) Equivalent simplified circuit of double-sided *LC* capacitive WPT system with a single gyrator.

fundamental harmonics approximation method [28] , the average value of the output current $I_{out,AVG}$ is found with the aid of the trans-conductance gain and the input voltage V_{in} as follows

$$I_{out,AVG} = \left| \frac{8}{\pi^2} \frac{\omega_0 C_P^* C_S^*}{C_M} V_{in} \right| . \quad (9)$$

Furthermore, the average output power $P_{out,AVG}$ can be expressed as

$$P_{out,AVG} = \left(\frac{8}{\pi^2} \frac{\omega_0 C_P^* C_S^*}{C_M} V_{in} \right)^2 \cdot R_{Load} . \quad (10)$$

To verify and demonstrate proof-of-concept of the behavioral model, a cycle-by-cycle simulation test-bench for the analyzed double-sided *LC* system has been constructed. The input voltage is 70V and the medium mutual capacitance C_M=3.5pF, at resonant frequency f_0≈1.55MHz. The resonant operation has been obtained with the following matching networks parameters: L_P =67μH, $C_P^* \approx C_P$ =156pF for the primary side, and L_S =90μH, $C_S^* \approx C_S$ =116pF for the secondary side. Simulation results of the currents and voltages of the primary and secondary are shown in Figs. 8a and 8b, respectively, for a load resistance R_{Load} =15Ω. The obtained peak values of the currents are in good agreement with the theoretical predications from (8), which further implies that the average output current, $I_{out,AVG}$, is as expected from (9).

Simulated and behavioral model average output current curves are shown in Fig. 9. In Fig. 9a the current is expressed as a function of the input voltage, and Fig. 9b depicts the

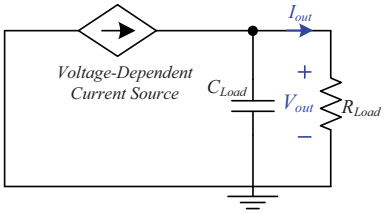

Fig. 7. Behavioral model of the analyzed capacitive WPT system.

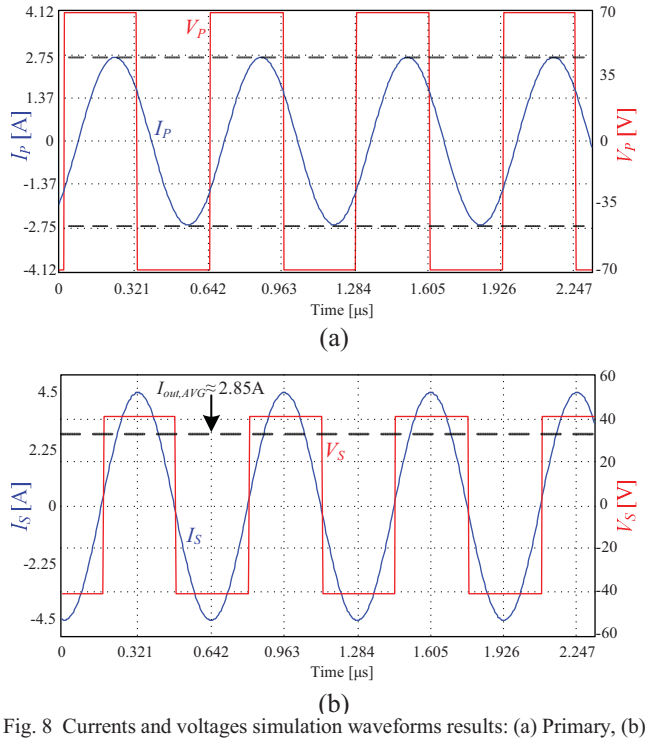

Fig. 8 Currents and voltages simulation waveforms results: (a) Primary, (b) Secondary.

output current for various medium coupling capacitances. As can be seen, the simulation results tightly follow the results obtained by the theoretical analysis of the behavioral model. From Fig. 9b it can be also noticed that the output current, and thus, the output power for the analyzed WPT system is inversely proportional to the mutual coupling capacitance C_M as mentioned in Section II.

IV. General Model Validation

To further validate and examine the behavioral model approach, an experimental double-sided *LC* capacitive WPT prototype with four copper plates that form the capacitive coupling has been constructed as shown in Fig. 10. The coupling plates have been designed symmetrically, such that each plate is 25x25cm. Thus, the matching networks have been also designed to be symmetrical, such that: L_P =L_S ≈67μH and C_P=C_S≈156pF. The gate drive signals of the full-bridge inverter were generated with a Cyclone IV FPGA at an operating frequency slightly above the resonance f_0 ≈1.56MHz guaranteeing soft-switching operation. The full-bridge inverter has been implemented with GaN power devices operable in several MHz [29]. To operate in the MHz range without any concern nor limitation due to magnetic and skin-effect losses [30] the matching inductors L_P and L_S have been constructed with a litz wire wrapped on an air-core. High-voltage multilayer SMD ceramic capacitors have been used for the matching capacitors C_P and C_S.

Fig. 11 shows experimental waveforms of the system for input voltage V_{in} =70V and a load resistance R_{Load} =15Ω,

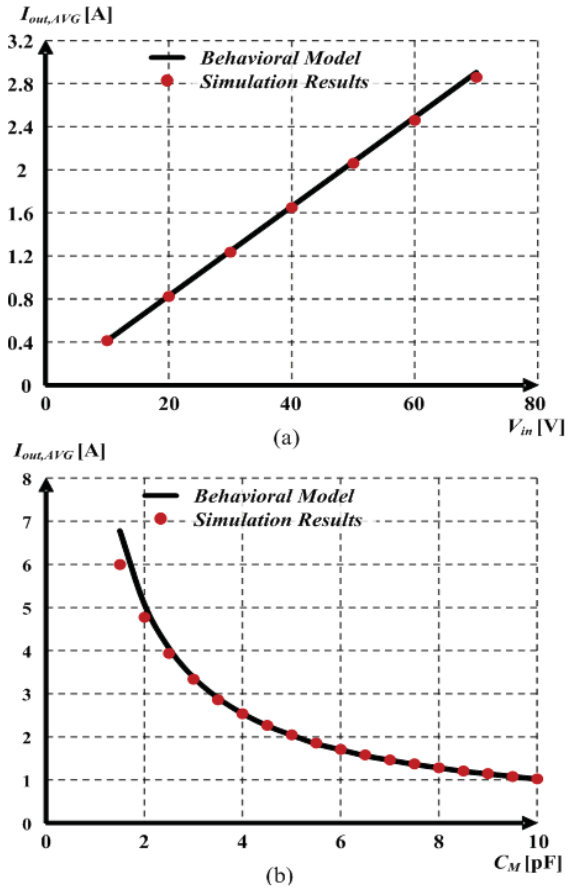

Fig. 9 Behavioral model and simulated average output current, $I_{out,AVG}$, curves: (a) As function of the input voltage V_{in}, (b) As a function of the mutual coupling capacitance C_M.

whereas the distance between the plates is approximately 5cm resulting in coupling capacitance $C_M \approx 6$pF. Fig. 11 a shows the primary sinusoidal current I_P, it can be noticed that the current is slightly lagging the primary voltage V_P validating soft-switching operation. It should be noted that to compensate for losses of the system to achieve the target output current, the input voltage has been adjusted slightly above 70V. The sinusoidal current at the secondary I_S is shown in Fig. 11 b. The obtained peak value (3.5A) as well as the resulting average value (2.25) at the secondary are in good agreement with behavioral model analysis given in (8) and (9). It should be emphasized that although the matching network at the secondary side is not perfectly tuned to the resonant frequency due to slight system variations, the experimental measurements follow the behavioral model predictions.

To further verify the strength of the behavioral model, the average output current has been measured for various input voltages and is summarized in Fig. 12. The experimental measurements tightly follow the results obtained by the simulations as well as the model predictions. It can be noticed that higher output current (as well as output power) is obtained for higher input voltage, as predicted from the gyrator current-voltage relationships that have been presented in Section III.

V. Conclusions

A two-port network based modeling approach for capacitive WPT systems has been presented. Based on the modeling approach, the behavior of capacitive WPT system can be analyzed and described for different system variations

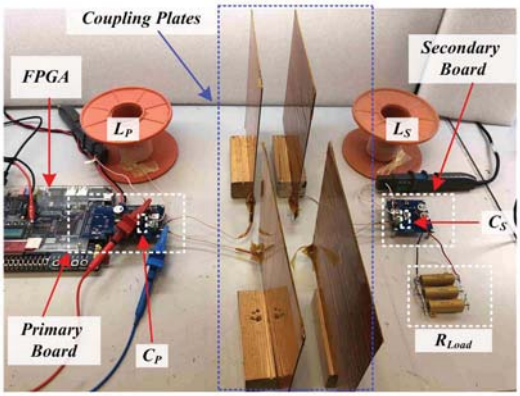

Fig. 10 Experimental setup of a double-sided *LC* capacitive WPT prototype.

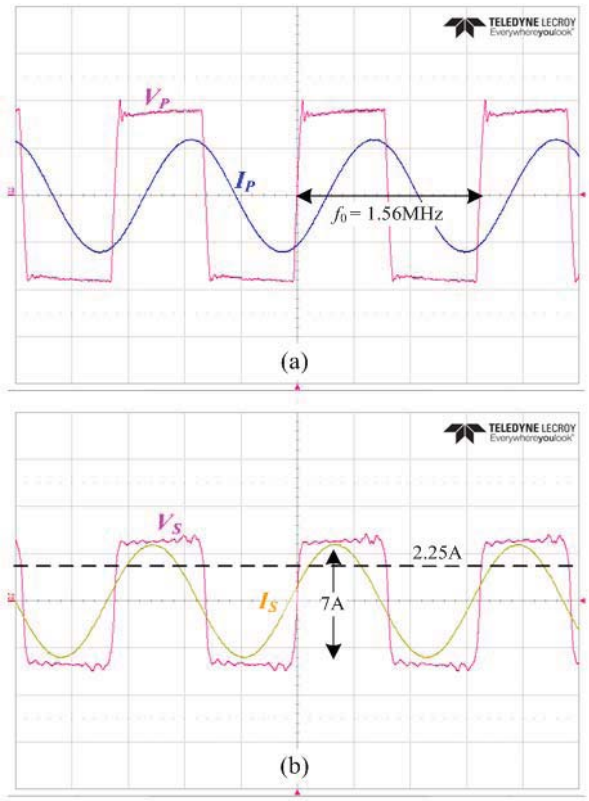

Fig. 11 Experimental waveforms with operating conditions: V_{in} =70V, R_{Load} =15Ω, coupling capacitance $C_M \approx 6$pF. (a) Primary side V_P 40V/div, I_P 3A/div, (b) Secondary side V_S 20V/div, I_S 3A/div. Time scale 200ns/div.

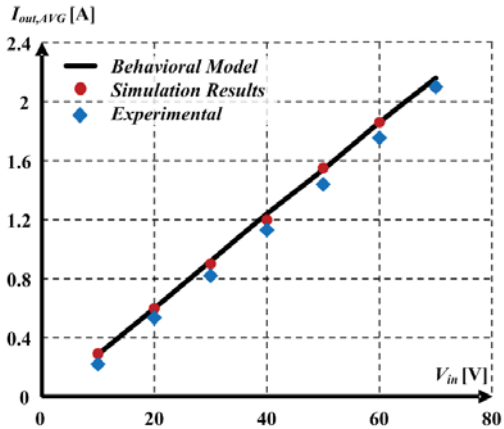

Fig. 12 Average output current, $I_{out,AVG}$, curve as function of the input voltage.

such as capacitive coupling interface, resonant frequency and matching networks components. The modeling method

provides an insight to the effects of the parameters on the system behavior, the cross-coupling relationships between transmitting and receiving sides, and sourcing features based on the operation mode and settings. The simplicity and generality of the gyrator model as an energy transfer element offers an efficient closed-form alternative to complex analytical approaches or tedious numerical simulations. The behavioral model and methodology have been validated through simulation and an experimental CPT prototype operating at 1.55 MHz under various operating conditions.

REFERENCES

[1] M. P. Theodoridis, "Effective capacitive power transfer," *IEEE Trans. Power Electron*., vol. 27, no. 12, pp. 4906–4913, Dec. 2012.

[2] F. Lu, H. Zhang, H. Hofmann, and C. Mi, "A double-sided LCLC compensated capacitive power transfer system for electric vehicle charging," *IEEE Trans. Power Electron.*, vol. 30, no. 11, pp. 6011–6014, Jun. 2015.

[3] H. Zhang, F. Lu, H. Hofmann, W. Liu, and C. C. Mi, "A four-plate compact capacitive coupler design and LCL-compensated topology for capacitive power transfer in electric vehicle charging application," *IEEE Trans. Power Electron*., vol. 31, no. 12, pp. 8541–8551, Dec. 2016.

[4] F. Lu, H. Zhang, H. Hofmann, C. Mi, "A loosely coupled capacitive power transfer system with LC compensation circuit topology," *Proc. IEEE Energy Convers. Congr. Expo. (ECCE)*, pp. 1-5, 2016.

[5] F. Lu, H. Zhang, C. Mi, "A two-plate capacitive wireless power transfer system for electric vehicle charging Applications," *IEEE Trans. Power Electron*, vol. 33, no. 2, pp. 946-969, Aug. 2017.

[6] F. Lu, H. Zhang, H. Hofmann, and C. Mi, "A double-sided LC compensation circuit for loosely-coupled capacitive power transfer," *IEEE Trans. Power Electron*., vol. 33, no. 2, pp. 1633 – 1643, Feb. 2017.

[7] T. Imura and Y. Hori, "Maximizing air gap and efficiency of magnetic resonant coupling for wireless power transfer using equivalent circuit and Neumann formula," *IEEE Trans. Ind. Electron*., vol. 58, no. 10, pp. 4746– 4752, Oct. 2011.

[8] J. Sallan, J. L. Villa, A. Llombart, and J. F. Sanz, "Optimal design of ICPT systems applied to electric vehicle battery charge," *IEEE Trans. Ind. Electron*., vol. 56, no. 6, pp. 2140–2149, Jun. 2009.

[9] S. Jaegue et al., "Design and implementation of shaped magnetic resonance-based wireless power transfer system for roadway-powered moving electric vehicles," *IEEE Trans. Ind. Electron*., vol. 61, no. 3, pp. 1179–1192, Mar. 2014.

[10] K. Wu, D. Choudhury, and H. Matsumoto, "Wireless power transmission, technology, and applications" *Proceedings of the IEEE*, Vol. 101, no.6, pp. 1271 – 1275, June 2013.

[11] L. Collins, "Cut the cord," *Electron. Syst. Softw.*, vol. 5, no. 6, pp. 42–46, Jan.–Dec. 2007.

[12] F. Lu, H. Zhang, H. Hofmann, C. Mi, "An inductive and capacitive integrated coupler and its LCL compensation circuit design for wireless power transfer," *IEEE Trans. Industry Applications*, vol. 53, no. 5, pp. 4903–4913, Oct. 2017.

[13] Y. Lim, H. Tang, S. Lim, J. Park, "An adaptive impedance-matching network based on a novel capacitor matrix for wireless power transfer," *IEEE Transactions on Power Electronics*, vol. 29, no. 8, pp. 4403-4413, August 2014.

[14] T.C. Beh, M. Kato, T. Imura, S. Oh and Y. Hori, "Automated impedance matching system for robust wireless power transfer via magnetic resonance coupling," *IEEE Transactions on Industrial Electronics*, vol. 60, no. 9, pp. 3689-3698, September 2013.

[15] W. Zhang and C. Mi, "Compensation topologies for high power wireless power transfer systems," *IEEE Transactions on Vehicular Technology*, vol. 65, no.6, pp. 4768-4778, July 2015.

[16] A. Kumar, S. Sinha, A. Sepahvand, K. K. Afridi, "Improved design optimization for high-efficiency matching networks," *IEEE Transactions on Power Electronics*, vol. 33, no. 1, pp. 37-50, Jan 2018.

[17] A. Witulski and R. W. Erickson, "Extension of state-space averaging to resonant switches and beyond," *IEEE Trans. Power Electron.*, vol. 5, no. 1, pp. 98–109, Jan. 1990.

[18] H. Hao, G. A. Covic, and J. T. Boys, "An approximate dynamic model of LCL-T-based inductive power transfer power supplies," *IEEE Trans. Power Electron*., vol. 29, no. 10, pp. 5554–5567, Oct. 2014.

[19] V. Vorperian, R. Tymerski, and F. C. Lee, "Equivalent circuit models for resonant and PWM switches," *IEEE Trans. Power Electron*., vol. 4, no. 2, pp. 205–214, Apr. 1989.

[20] D. Maksimovic and S. Cuk, "A unified analysis of PWM converters in discontinuous modes," *IEEE Trans. Power Electron.*, vol. 6, no. 3, pp. 476–490, Jul. 1991.

[21] J. Lu, A. Kumar, K. K. Afridi, "A step-superposition based analysis approach to modeling resonant converters," *IEEE Trans. Power Electron*., vol. 33, no. 8, pp. 7148-7165, Aug. 2018.

[22] C. J. Anderson and J. A. Lyle, "Technique for evaluating system performance using Q in numerical simulation exhibiting inter symbol interference," *Electron. Lett*., vol. 30, pp. 71–72, 1994.

[23] L. Chen, S. Liu, Y. Zhou, and T. Cui, "An optimizable circuit structure for high-efficiency wireless power transfer," *IEEE Trans. Ind. Electron.*, vol. 60, no. 1, pp. 339–349, Jan. 2013.

[24] B. Wang, W. Yerazunis, and K. H. Teo, "Wireless power transfer: Metamaterials and array of coupled resonators," in *Proc. IEEE*, vol. 101, no. 6, pp. 1359–1368, Jun. 2013.

[25] Y. H. Sohn, B. H. Choi, G. H. Cho, and C. T. Rim, "Gyrator-Based Analysis of Resonant Circuits in Inductive Power Transfer Systems," *IEEE Transactions on Power Electronics*, vol. 31, no. 10, pp. 6824-6843, Oct. 2016.

[26] S. Singer, "Loss-free gyrator realization," *IEEE Transactions on Circuits and Systems,* vol. 35, no. 1, pp. 26-34, Jan. 1988.

[27] S. Singer, "Gyrators application in power processing circuits," *IEEE Trans. Ind. Electron*., vol. IE-34, no. 3, pp. 313–318, Aug. 1987.

[28] R.L. Steigerwald, "A Comparison of Half-Bridge Resonant Converter Topologies," *IEEE Transactions on Power Electronics*, vol. 3, no. 2, pp. 174-182, April 1988.

[29] Texas Instrument: 'LMG5200 80-V, 10-A GaN Half-Bridge Power Stage' available at: http://www.ti.com/lit/ds/symlink/lmg5200.pdf, accessed March 2017.

[30] M. Bartoli, N. Noferi, A. Reatti, and M. Kazimierczuk, "Modeling litzwire winding losses in high-frequency power inductors," in *Proc. IEEE Power Electronics Specialists Conf*., Jun. 23–27, 1996, pp. 1690–1696.